



## Enhanced strength and plasticity of a Ti-based metallic glass at cryogenic temperatures

Yongjiang Huang<sup>a</sup>, Jun Shen<sup>a,\*</sup>, Jianfei Sun<sup>a</sup>, Zhefeng Zhang<sup>b,\*</sup>

<sup>a</sup> School of Materials Science and Engineering, Harbin Institute of Technology, Harbin 150001, China

<sup>b</sup> Shenyang National Laboratory for Materials Science, Institute of Metal Research, Chinese Academy of Sciences, Shenyang 110016, China

### ARTICLE INFO

#### Article history:

Received 31 January 2008

Received in revised form 2 July 2008

Accepted 7 August 2008

#### Keywords:

Metallic glasses

Mechanical properties

Cryogenic temperatures

Shear bands

Plasticity

### ABSTRACT

Conventional crystalline materials usually exhibit a ductile to brittle transition behaviour at low temperatures. An increase in the strength is always accompanied by a decrease in the plasticity. Here the authors report on a significant enhancement in both compressive strength and plasticity of a Ti-based bulk metallic glass (BMG) deformed at low temperatures. The ductilization of the BMG system can be evidently attributed to the formation of dense shear bands and the rotation mechanism of shear bands. The cryogenic surroundings can effectively slow down the mobility and diffusion of the atoms and consequently, suppress the nucleation and growth of nanocrystals during the deformation process, allowing the simultaneous improvement in the mechanical responses of the glassy alloy to compressive loading far below the ambient temperature.

© 2008 Elsevier B.V. All rights reserved.

### 1. Introduction

Since their discovery around 1960, metallic glasses have attracted considerable interest because of a combination of excellent properties, including high strength, high hardness, and high resistance to corrosion [1–3]. Unfortunately, these properties can not be fully exploited due to their brittle fracture behaviours. Without crystalline structure, dislocation contribution to ductile deformation is impossible for amorphous alloys. Although large ductility has been observed recently in a few bulk metallic glasses (BMG) [4–9], deformation in amorphous alloys takes place only in a few, highly localized shear bands, leading to remarkably little plastic strain of <2% in compression and nearly zero plastic strain in tension at room temperature, which limits their widespread applications as promising structural materials [10]. To improve the plastic deformation capability of BMGs, numerous efforts have focused on the preparation of BMG-based composites by introducing the second crystalline phase or by in situ formation of crystalline phase [11–14]. Very recently, a few approaches have been proposed to develop simple and feasible methods that could enhance the plasticity of the BMGs including the known BMG systems [15–17].

Research on the plastic deformation of metallic materials at low temperatures is extremely topical in order to obtain high quality

structural materials for cryogenic techniques. Common crystalline metals with bcc or hcp structure have a ductile to brittle transition temperature, below which the materials become very brittle [18]. For fcc metals and alloys, ductility can be maintained at low temperature due to a uniform and efficient storage of dislocation [18]. Several recent studies have shown that both the strength and the ductility of some nano-structured materials increase with decreasing testing temperatures [19,20]. It remains uncertain whether metallic glasses become ductile or brittle at cryogenic temperatures so far. There are only few reports about the low-temperature mechanical behaviours of metallic glasses, and the plasticity of those BMGs at cryogenic temperatures was not distinctly improved, albeit certain increase in strength was found [18,21–24]. In this paper, we report a remarkable enhancement in both strength and plasticity of the  $\text{Ti}_{40}\text{Zr}_{25}\text{Ni}_3\text{Cu}_{12}\text{Be}_{20}$  (at.%) bulk metallic glass deformed at cryogenic temperatures. A comparison is made to demonstrate the striking temperature dependence of the mechanical properties of the studied alloy.

### 2. Experiments

The  $\text{Ti}_{40}\text{Zr}_{25}\text{Ni}_3\text{Cu}_{12}\text{Be}_{20}$  (at.%) alloy ingots were prepared by arc-melting elemental pieces with purity above 99.9% and casting into the copper mould under a purified Ar atmosphere. The resulting rod shaped samples have a diameter of 3 mm and a length of 30 mm. The glassy nature of as-prepared alloy rods was verified by using X-ray diffraction (not shown). From the as-cast rods, cylindrical specimens with an aspect ratio of 2:1 were prepared

\* Corresponding authors. Tel.: +86 451 86403196; fax: +86 451 86403196.

E-mail addresses: [junshen@hit.edu.cn](mailto:junshen@hit.edu.cn) (J. Shen), [zhfzhang@imr.ac.cn](mailto:zhfzhang@imr.ac.cn) (Z. Zhang).

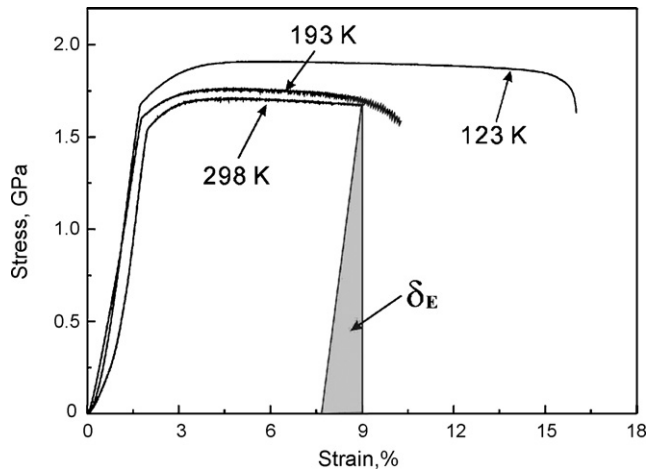


Fig. 1. Compressive stress–strain curves of the alloy tested at 298 K, 193 K, and 123 K.

for compression tests. The ends of all the specimens were carefully polished to make them parallel to each other. The uniaxial compression tests were conducted at 298 K, 193 K, and 123 K on an Instron 5500 mechanical instrument with a constant cross-head speed to produce an initial strain rate of  $4 \times 10^{-4} \text{ s}^{-1}$ . Liquid nitrogen was used for cryostating. Following compression tests, the fracture surface morphology and the fracture features were investigated using scanning electron microscope (SEM). Thermal properties of the fractured specimens as well as the as-cast specimen were measured with differential scanning calorimetry (DSC) using a continuous heating rate of 20 K/min.

### 3. Results and discussion

Fig. 1 presents the compressive engineering stress–strain curves for the Ti-based BMG tested at 298 K, 193 K, and 123 K. The compressive properties of the alloy at different temperatures, including the yield strength  $\sigma_y$ , the maximum fracture strength  $\sigma_m$ , and the plastic strain  $\varepsilon_p$ , are listed in Table 1. It can be seen that the Ti-based BMG exhibits both high strength and high plasticity not only at room temperature, but also at low temperatures. The high plasticity of the Ti-based BMG deformed at room temperature is quite similar to the previous results [25–27]. In particular, both the strength and the plasticity of the Ti-based alloy increase with decreasing the testing temperatures without a ductile to brittle transition. However, the significantly high plasticity exhibited at low temperatures has never been observed for other BMGs [21–24]. The simultaneous enhancement in both strength and plasticity at low temperatures conflicts with the traditional trend of the strength–plasticity relationship for crystalline materials, i.e., an increase in the strength is always accompanied by a decrease in the plasticity, and vice versa. Recently, it is found that the strength of metallic glasses follows the below relation [21]

$$\sigma = aE \left( \frac{b - T}{T_g} \right) \quad (1)$$

Table 1

Yield strength  $\sigma_y$ , maximum fractured strength  $\sigma_m$ , plastic strain  $\varepsilon_p$ , shear fracture angle  $\theta_c^F$ , and the initial shear angle of the primary shear bands  $\theta_c^0$  for the studied alloy compression deformed at 298 K, 193 K, and 123 K

Testing conditions	$\sigma_y$ (MPa)	$\sigma_m$ (MPa)	$\varepsilon_p$ (%)	$\theta_c^F$ (°)	$\theta_c^0$ (°)
298 K, $4 \times 10^{-4} \text{ s}^{-1}$	1583	1710	6.9	41.5	39.8
193 K, $4 \times 10^{-4} \text{ s}^{-1}$	1633	1761	8.6	42.5	40.2
123 K, $4 \times 10^{-4} \text{ s}^{-1}$	1711	1908	14.5	43.5	39.6

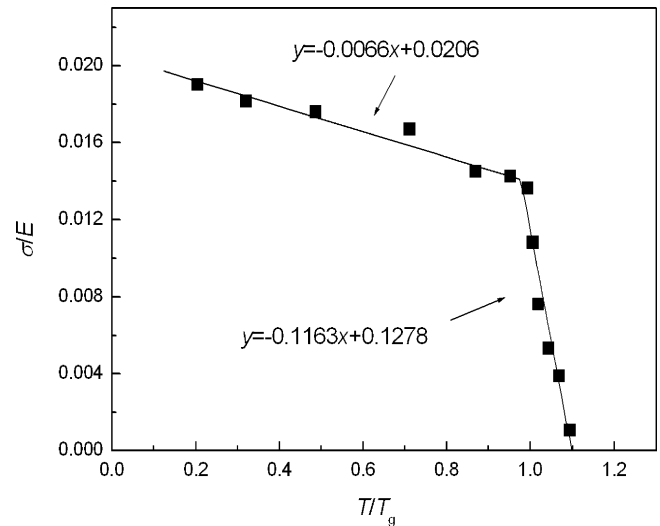
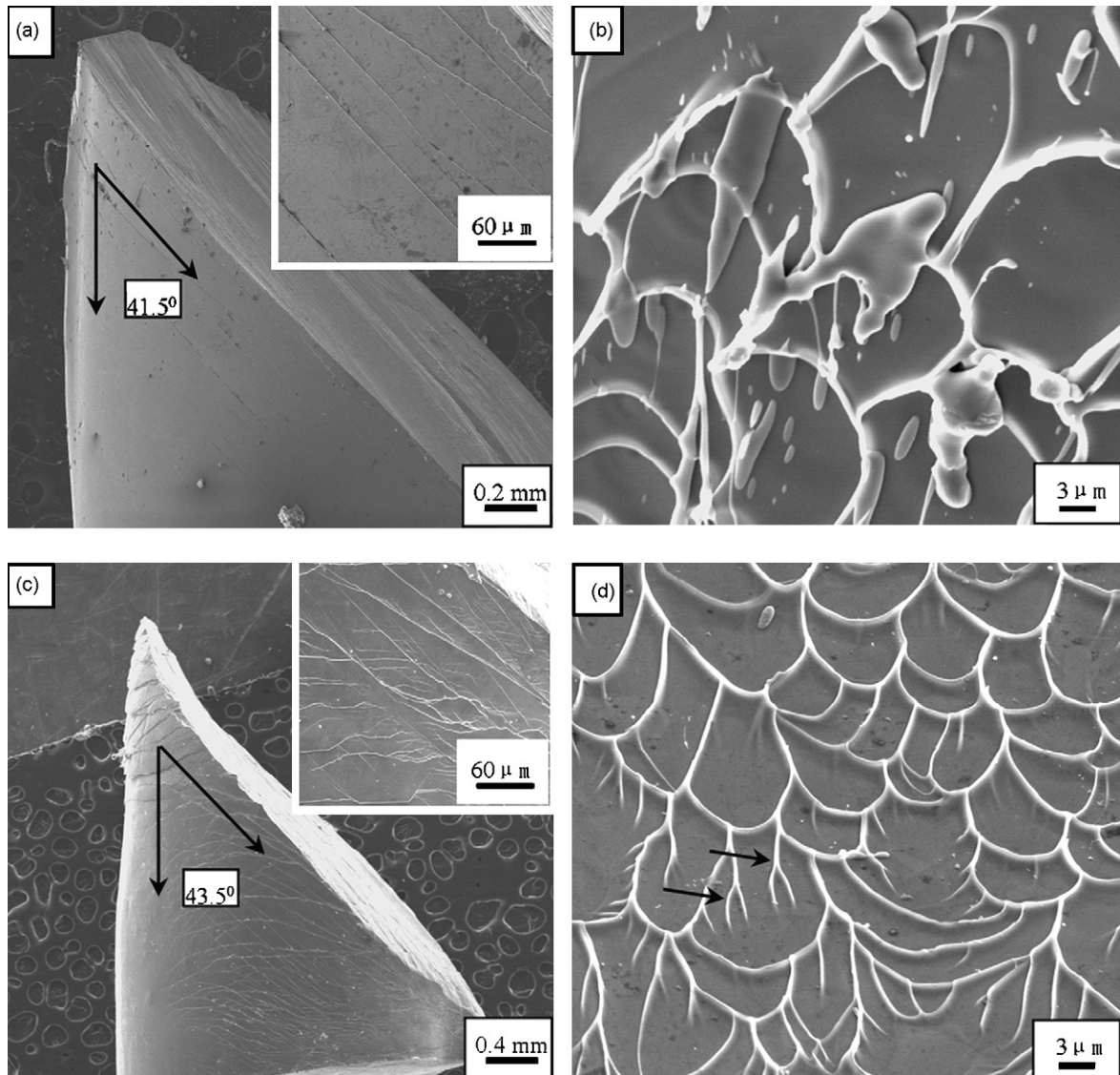


Fig. 2. The normalized temperature ( $T/T_g$ ) dependence of the normalized strength ( $\sigma/E$ ) for the studied alloy.

where  $T$  is the testing temperature,  $T_g$  is the glass transition temperature,  $E$  is the Young's modulus, and  $a$  and  $b$  are two constants of the metallic glass. The temperature dependence of the strength for the amorphous  $\text{Ti}_{40}\text{Zr}_{25}\text{Ni}_3\text{Cu}_{12}\text{Be}_{20}$  alloy is shown in Fig. 2. It is apparent that, following the relation revealed in Eq. (1), the strength of the Ti-based metallic glass increases with decreasing testing temperature, which is consistent with the previous reports [21–24].

Fig. 3(a) and (c) shows the typical shear fracture behaviour of the specimens. It is found that the shear fracture surfaces orient at an angle of about  $41.5^\circ$ ,  $42.5^\circ$ , and  $43.5^\circ$ , respectively, to the loading axis for the specimens deformed at 298 K, 193 K and 123 K, as listed in Table 1. Further observations demonstrate that there are dense shear bands near the fractography of the specimens, which must contribute the high plasticity of the Ti-based BMG at the testing temperatures. Normally, the shear bands are straight and well-separated on the surface of the specimen deformed at 298 K, as inset in Fig. 3(a). In contrast, for the fracture surface of the specimen deformed at 123 K, one can notice the occurrence of branching of individual shear bands as they propagate through the material (inset in Fig. 3(c)). It is obvious that the compressive shear fracture angles, accompanying the plasticity, slightly increase as the testing temperature decreases. Zhang et al. [28] presented a rotation mechanism of the primary shear bands due to a high compressive plasticity to explain the shear fracture mode of Ti-based nano-structured materials and established a relationship among the initial shear angle  $\theta_c^0$  of the primary shear bands, the shear fracture angle  $\theta_c^F$  and the plastic strain  $\varepsilon_p$ , i.e.,  $\sin(\theta_c^0) = \sqrt{1 - \varepsilon_p} \sin(\theta_c^F)$ . This model allows us to estimate the initial shear angles  $\theta_c^0$  of the primary shear bands by incorporating the experimentally available data of  $\varepsilon_p$  and  $\theta_c^F$ . As listed in Table 1, all  $\theta_c^0$  for the fractured specimens are quite close to  $\sim 40^\circ$ . This result agrees well with the previous observations at room temperature for other glassy alloys [10,28–30], indicating that the fracture of the alloy at low temperatures still follows the Mohr–Coulomb criterion. The rotation of primary shear bands provides a good indicator of enhancement in plasticity of the Ti-based alloy at low temperatures.

Metallic glasses with amorphous structure lack lattice order; their plastic deformation is mainly dominated by the initiation and propagation of shear bands [31–33]. When compressing a BMG specimen, yielding always accompanies the shear-band formation; and the continuous propagation of the shear bands is associated



**Fig. 3.** SEM images showing the outer shapes of the specimen deformed at 298 K (a); 123 K (c) and the fracture surfaces of the specimens deformed at 298 K (b) and 123 K (d).

with the atomic-scale free-volume zones [31–33], leading to a macroscopic plastic deformation, as shown in Fig. 3. Within shear bands, the severe localized plastic deformation at high shear stress (in  $\sim$ GPa level) must generate heat, resulting in the local temperature rise in the shear-deformation zones [34,35]. At 123 K, the cryogenic environment can partially relieve the local heat ahead of the shear-band tip. As a result, the propagation of the shear bands may become more difficult at cryogenic temperatures. Meanwhile, the inhibited motion of the shear bands could either facilitate the generation of more shear bands or cause certain rotation of the shear bands. Indeed, the SEM observations have demonstrated that the specimen fractured at 123 K shows more shear bands and serious shear rotation than that fractured at 298 K, as shown in Fig. 3.

On the other hand, the local temperature rise resulting from the adiabatic shear can prompt the advancement of shear bands, which, in turn, often causes the disappearance of the work-hardening of the BMGs [22–24,29,30]. According to Eq. (1), the temperature within the shear-deformation zone might be associated with the glass transition temperature  $T_g$ . When the shear-deformation zone can not support the high applied stress, the catastrophic failure

always starts to occur along the main shear-band with severe plastic deformation [29–33]. A study of the morphology of fracture surfaces revealed characteristic vein-like patterns and droplet features on all surfaces of the shear fractured specimens, as shown in Fig. 3(b) and (d). It is apparent that the droplets formed at 123 K are much smaller and more homogeneous than those formed at 298 K. At the same time, we can notice that the fracture surface of the specimen deformed at 298 K exhibits full finger veins while the fracture surface of the specimen deformed at 123 K exhibits a lot of tributary veins (as marked by arrows in Fig. 3(d)) besides some full finger veins.

In the fracture process of metallic glasses, the formation of vein-like patterns is attributed to a significant reduction in viscosity in the shear bands before catastrophic failure of the specimen [34,35]. The large amount of heat induced melting on the fracture surface originates from the instantaneous release of the stored elastic energy during fracture of the BMGs [34,35]. This requires two necessary conditions. First, the materials must be strong enough (i.e., exhibit a high strength) to store a significant amount of elastic energy from the applied load. Second, the stored elastic energy in

the materials must dissipate heat into a small volume fraction of the specimen during the fracture. The two requirements are just satisfied for BMG materials. As shown in Fig. 1, the area of the triangle in the stress–strain curve represents the elastic energy  $\delta_e$  stored in the material before failure, i.e.,

$$\delta_e = \frac{V_0 \sigma_m^2}{2E} \quad (2)$$

where  $V_0$  is the volume of the specimen. Quantitatively, the enthalpy,  $\delta_h$ , needed for melting the local shear layer of the BMG specimen from  $T_g$  can be calculated by the following equation

$$\delta_h = \rho C_p (T_f - T_g) V_0 \eta \quad (3)$$

Herein,  $T_f$  is the final temperature of the shear layer and is higher than the melting point,  $C_p$  is the specific heat capacity,  $\rho$  is the density and  $\eta$  is the percentage of the melting volume. Assuming that all the elastic energy  $\delta_e$  is transformed into the heat  $\delta_h$  to melt the shear layer during the rapid fracture, one can get

$$(T_f - T_g) = \frac{\sigma_m^2}{2\eta E \rho C_p} \quad (4)$$

Also assuming that the thickness of shear melting layer of the BMG is the same for the specimens failed at the temperatures of 298 K and 123 K, the final temperatures  $T_f^{298}$  and  $T_f^{123}$  of the two shear layers have the following relation,

$$\frac{(T_f^{123} - T_g)}{(T_f^{298} - T_g)} = \left( \frac{\sigma_m^{123}}{\sigma_m^{298}} \right)^2 \quad (5)$$

Substituting  $\sigma_m^{298} = 1710$  MPa and  $\sigma_m^{123} = 1908$  MPa into Eq. (4), one can get

$$T_f^{123} = T_f^{298} + 0.25(T_f^{298} - T_g) > T_f^{298} \quad (6)$$

This indicates that the final temperature  $T_f^{123}$  within the shear fracture layer of the specimen at 123 K is higher than that ( $T_f^{298}$ ) at 298 K. Thus, the viscosity of the viscous medium within the shear melting layer increases significantly with the decrease in temperature. Meanwhile, the rapid shear fracture of the specimen at 123 K has undergone a relatively high average normal stress than that at 298 K. Therefore, it is reasonable that, for the specimens deformed at 123 K, the lower viscosity of the viscous medium within the shear melting layer and the higher applied normal stress can lead to more homogeneous distribution of the molten droplets with a smaller size and the well developed vein patterns with bifurcated structure on the fracture surface, as observed in Fig. 3(d), compared with the fracture patterns for the specimen deformed at room temperature, as shown in Fig. 3(b).

It has been established that presence of cluster or nanocrystals with proper size and volume fraction in amorphous matrix favours the ductilization of a BMG alloy. In order to examine the effect of deformation on the formation of nanocrystals, we conducted DSC measurements on the as-cast specimen and deformed specimens. As shown in Fig. 4, all specimens exhibit an endothermic event, characteristic of glass transition, followed by two exothermic peaks representing a two-step crystallization event. The amplitudes of the crystallization associated heat flow (see the inset in Fig. 4) for the deformed specimens are less than that for the as-cast specimen, revealing that deformation-induced crystallization occurs. Moreover, compared with the specimen deformed at room temperature (298 K), the specimen deformed at low temperature (123 K) exhibits a lower loss in crystallization heat with respect to the undeformed, as-cast specimen, suggesting that the crystallization in the low temperature deformed specimen is not as profound as the crystallization in the room temperature deformed

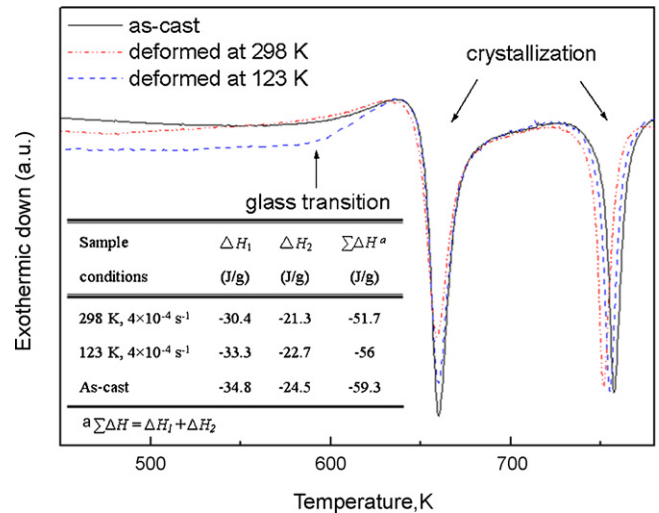


Fig. 4. DSC curves obtained from the deformed specimens as well as the as-cast specimen. Inset shows the heat flow associated with the first ( $\Delta H_1$ ) and second ( $\Delta H_2$ ) stage crystallization.

specimen. Since amorphous alloys are not in thermodynamic equilibrium, supplying such alloys with sufficient mechanical energy can promote a phase transformation from an amorphous solid to a more stable crystalline phase [36–38]. During plastic deformation of metal glasses, atomic dilatation occurs due to the localization of the high plastic strain [38]. A large proportion of atoms are subjected to local displacements, which will lead to the enhancement of the atomic diffusion mobility and atomic rearrangement, promoting crystallization in metal glasses [38]. On the other hand, the local heating within the shear bands occurs during plastic deformation. Such heating can also cause the crystallization of the glassy metal near shear bands to some extent. As a result, crystallization induced by uniaxial compression does take place for the studied alloy deformed at both 298 K and 123 K. Under low temperature surroundings, atomic dilatation is inhibited, reducing the crystallization of amorphous alloys. Accordingly, the exothermic enthalpies of the specimen deformed at 123 K are less than that for the specimen deformed at 298 K, favoring the simultaneous enhancement in the strength and plasticity of the glassy alloy at low temperature by suppressing either initial precipitation or subsequent growth of crystalline phases.

#### 4. Conclusions

We discovered that the Ti-based BMG possesses very high strength and good plasticity not only at room temperature, but also at low temperatures. In particular, the simultaneous improvement in both strength and plasticity at low temperatures conflicts with the traditional trend of the strength–plasticity relationship for crystalline materials. The high plasticity of the Ti-based BMG can be attributed to the formation of dense shear bands. With decreasing the testing temperature, the propagation of the shear bands may be more difficult and a large number of branched shear bands form during fracture, leading to improved plasticity of the metallic glass at lower temperatures. This indicates that the Ti-based BMG possesses intrinsic ductile nature, which provides a new strategy to fabricate high-performance structural materials.

#### Acknowledgements

This work was supported by the Program for New Century Excellent Talents in University (China), the National Natural Sci-

ence Foundation of China (NSFC) under grant nos. 50771040 and 10732010, and the Hi-Tech Research and Development Program of China (project no.: 2007AA03Z518) (J. Shen) and NSFC under grant nos. 50401019 and 50625103, and the “Hundred of Talents Project” by Chinese Academy of Sciences (Z.F. Zhang).

## References

- [1] W. Klement, R.H. Willens, P. Duwez, *Nature* 187 (1960) 869–870.
- [2] A.L. Greer, *Science* 267 (1995) 1947–1953.
- [3] A. Inoue, *Acta Mater.* 48 (2000) 279–306.
- [4] J. Schroers, W.L. Johnson, *Phys. Rev. Lett.* 93 (2004) 255506.
- [5] F.Q. Guo, H.J. Wang, S.J. Poon, G.J. Shiflet, *Appl. Phys. Lett.* 86 (2005) 091907.
- [6] J. Das, M.B. Tang, K.B. Kim, R. Theissmann, F. Baier, W.H. Wang, J. Eckert, *Phys. Rev. Lett.* 94 (2005) 205501.
- [7] L.Q. Xing, Y. Li, K.T. Ramesh, J. Li, T.C. Hufnagel, *Phys. Rev. B* 64 (2001) 180201.
- [8] J.C. Oh, T. Ohkubo, Y.C. Kim, E. Fleury, K. Hono, *Scripta Mater.* 53 (2005) 165–169.
- [9] Y.H. Liu, G. Wang, R.J. Wang, D.Q. Zhao, M.X. Pan, W.H. Wang, *Science* 315 (2007) 1385–1388.
- [10] Z.F. Zhang, J. Eckert, *Phys. Rev. Lett.* 94 (2005) 094301.
- [11] C.C. Hays, C.P. Kim, W.L. Johnson, *Phys. Rev. Lett.* 84 (2000) 2901–2904.
- [12] R.D. Conner, R.B. Dandliker, W.L. Johnson, *Acta Mater.* 46 (1998) 6089–6102.
- [13] M.L. Lee, Y. Li, C.A. Schuh, *Acta Mater.* 52 (2004) 4121–4131.
- [14] D.C. Hofmann, J.-Y. Suh, A. Wiest, G. Duan, M.-L. Lind, M.D. Demetriou, W.L. Johnson, *Nature* 451 (2008) 1085–1089.
- [15] Y. Zhang, W.H. Wang, A.L. Greer, *Nat. Mater.* 5 (2006) 857–860.
- [16] P. Yu, Y.H. Liu, G. Wang, H.Y. Bai, W.H. Wang, *J. Mater. Res.* 22 (2007) 2384–2388.
- [17] L.Y. Chen, Q. Ge, S. Qu, Q.K. Jiang, X.P. Nie, J.Z. Jiang, *Appl. Phys. Lett.* 92 (2008) 211905.
- [18] C. Fan, H. Li, L.J. Kecskes, K. Tao, H. Choo, P.K. Liaw, C.T. Liu, *Phys. Rev. Lett.* 96 (2006) 145506.
- [19] Y.M. Wang, E. Ma, *Appl. Phys. Lett.* 83 (2003) 3165–3167.
- [20] Y.M. Wang, E. Ma, *Acta Mater.* 52 (2004) 1699–1709.
- [21] H. Li, C. Fan, K. Tao, H. Choo, P.K. Liaw, *Adv. Mater.* 18 (2006) 752–754.
- [22] C.A. Pampillo, D.E. Polk, *Acta Metall.* 22 (1974) 741–749.
- [23] S. Takeuchi, T. Kakegawa, T. Hashimoto, A.P. Tsai, A. Inoue, *Mater. Trans.* 41 (2000) 1443–1447.
- [24] V.Z. Bengus, E.D. Tabachnikova, J. Miskuf, K. Csach, V. Ocelik, W.L. Johnson, V.V. Molokanov, *J. Mater. Sci.* 35 (2000) 4449.
- [25] H. Men, S.J. Pang, A. Inoue, T. Zhang, *Mater. Trans.* 46 (2005) 2218–2220.
- [26] J.M. Park, H.J. Chang, K.H. Han, W.T. Kim, D.H. Kim, *Scripta Mater.* 53 (2005) 1–6.
- [27] Y.C. Kim, J.H. Na, J.M. Park, D.H. Kim, J.K. Lee, W.T. Kim, *Appl. Phys. Lett.* 83 (2003) 3093–3095.
- [28] Z.F. Zhang, G. He, H. Zhang, J. Eckert, *Scripta Mater.* 52 (2005) 945–949.
- [29] W.J. Wright, R.B. Schwarz, W.D. Nix, *Mater. Sci. Eng. A* 319–321 (2001) 229–232.
- [30] Z.F. Zhang, J. Eckert, L. Schultz, *Acta Mater.* 51 (2003) 1167–1179.
- [31] F. Spaepen, *Acta Metall.* 25 (1977) 407–415.
- [32] A.S. Argon, *Acta Metall.* 27 (1979) 47–58.
- [33] P.E. Donovan, W.M. Stobbs, *Acta Metall.* 29 (1981) 1419–1436.
- [34] J.J. Lewandowski, A.L. Greer, *Nat. Mater.* 5 (2006) 15–18.
- [35] F. Spaepen, *Nat. Mater.* 5 (2006) 7–8.
- [36] H. Chen, Y. He, G.J. Shiflet, S.J. Poon, *Nature* 367 (1994) 541–543.
- [37] J.J. Kim, Y. Choi, S. Suresh, A.S. Argon, *Science* 295 (2002) 654–657.
- [38] S.W. Lee, M.Y. Huh, S.W. Chae, J.C. Lee, *Scripta Mater.* 54 (2006) 1439–1444.